The Effects of Phase Transformation on the Structure and Mechanical Properties of TiSiCN Nanocomposite Coatings Deposited by PECVD Method

Mohammad Abedi[1], Amir Abdollah-zadeh[*,1], Massimiliano Bestetti[2], Antonello Vicenzo[2], Andrea Serafini[2], Farid Movassagh-Alanagh[1]

[1]Department of Materials Eng., Tarbiat Modares University, P.O. Box 14115-143, Tehran, Iran

[2] Department of Chemistry, Materials and Chemical Engineering "Giulio Natta", Politecnico di Milano, 20131 Milano, Italy

Abstract

In the present study, the effects of phase transformations on the structure and mechanical properties of TiSiCN coatings were investigated. TiSiCN nanocomposite coatings were deposited on AISI H13 hot-work tool steel by a pulsed direct current plasma-enhanced chemical vapor deposition process at 350 or 500 °C, using $TiCl_4$ and $SiCl_4$ as the precursors of Ti and Si, respectively, in a $CH_4/N_2/H_2$/Ar plasma as the source of carbon and nitrogen and reducing environment. Some samples deposited at 350 °C were subsequently annealed at 500 °C under Ar atmosphere. Super hard self-lubricant TiSiCN coatings, having nanocomposite structure consisting of TiCN nanocrystals and amorphous carbon particles embedded in an amorphous $SiCN_x$ matrix, formed through spinodal decomposition in the specimens deposited or annealed at 500 °C. In addition, it was revealed that either uncomplete or relatively coarse phase

[*]Mail of corresponding author: zadeh@modares.ac.ir

Tel&Fax:+982182885040

segregation of titanium compounds was achieved during deposition at 350 °C and 500 °C, respectively. On the contrary, by deposition at 350 °C followed by annealing at 500 °C, a finer structure was obtained with a sensible improvement of the mechanical properties of coatings. Accordingly, the main finding of this work is that significant enhancement in key properties of TiSiCN coatings, such as hardness, adhesion and friction coefficient, can be obtained by deposition at low temperature and subsequent annealing at higher temperature, thanks to the formation of a fine grained nanocomposite structure.

Keywords: PECVD, Tribological coatings, TiSiCN, Nanocomposite microstructure, Spinodal hardening.

1. Introduction

Wear resistant hard coatings based on transition metal nitrides and carbo-nitrides are widely used to increase the lifetime of forging and extrusion dies and of high-speed machining tools. Over the past two decades, the widespread adoption of these coatings has encouraged and sustained the development of new processes and materials in the attempt to further improve their properties [1]. Among these coatings, the higher hardness, excellent oxidation resistance and high thermal stability of nanocomposite films [2], such as TiSiN [3-5] and TiSiCN [6, 7], make them the most promising candidates for highly demanding tribological applications. The nanocomposite structure of TiSiN and TiSiCN coatings results from the formation of an amorphous (*a*) matrix of Si_3N_4 or $SiCN_x$, respectively, embedding finely dispersed nanocrystalline (*nc*) second phases, such as TiN or TiCN [8]. In the case of TiSiCN coatings, the carbon in excess over the stoichiometric composition of the matrix and crystalline particles

will separate and disperse in the matrix as amorphous carbon or diamond like carbon (DLC) particles [6, 8], thus imparting low friction properties to the surface.

Either chemical vapor deposition (CVD) [6-9] or physical vapor deposition (PVD) [10, 11] techniques can be used to synthesize TiSiCN coatings. Plasma-enhanced chemical vapor deposition (PECVD) [6, 8, 9], due to its notable characteristics and capabilities, such as relatively low deposition temperature and high working pressure, adequate coating to substrate adhesion, and excellent step coverage, is widely applied by researchers and in the industry. PECVD processes for the deposition of TiSiCN coatings, in this respect similar to TiSiN [12], operate at temperature typically in the range from 500 to 600 °C [6, 8, 9], thereby imposing obvious restrictions on the industrial use of these coatings, in particular making unpractical the deposition on tool steel parts. However, in the light of the general understanding of nanocomposite structure generation based on spinodal phase segregation [13], the growth temperature is recognized as a key parameter controlling nanocomposite formation and affecting its microstructural characteristics. Actually, the slowing down of diffusion processes resulting from lowering the deposition temperature, below about 500 °C according to Věprek [13], would severely inhibit the kinetics of the spinodal phase segregation process. Accordingly, a low temperature PECVD process would not appear to be a feasible approach for the synthesis of TiSiCN nanocomposite, unless followed by annealing at temperature high enough for the spinodal hardening process to occur. There are only a few instances where a similar processing strategy has been attempted with nanocomposites, such as ($Al_{1-x}Ti_x$) N/a- Si_3N_4 [14] and TiAlSiN [15], also in view of enhancing the coating-substrate adhesion. Accordingly, the primary objective of the present work was to investigate the effects of annealing on TiSiCN self-lubricant nanocomposite coatings deposited on AISI H13 steel substrate via pulsed-DC PECVD. The deposition was performed at two different temperatures of 350 and 500 °C, and samples deposited at 350 °C were subsequently annealed at 500 °C to investigate the structural

changes due to spinodal decomposition and its effects on the mechanical properties of the coatings.

2. Materials and methods

2.1. Deposition and annealing of coatings

TiSiCN coatings were deposited on mirror finished AISI H13 substrates by direct current pulsed PECVD, using a gaseous mixture of H_2 (flow rate of 200 sccm), Ar (100 sccm), N_2 (40 sccm), CH_4 (5 sccm), $TiCl_4$ (5 sccm) and $SiCl_4$ (1 sccm). A Plasma Fanavar Amin (PFA) Co. (Iran) direct current PECVD system was used and operated under a pulsed direct potential difference of 650 V, with a frequency of 12 kHz and duty cycle of 33%. The potential difference was applied between the chamber wall, the anode, and the substrate stage, the cathode. The deposition process was performed at either 350 °C or 500 °C for 3 hours. The wall of the chamber was heated by heating elements and the temperature was monitored using a thermocouple (Pt-Pt 10% Rh) embedded into a sample on the stage. After deposition, samples were left to cool to room temperature in the vacuum chamber (5×10^{-3} torr) during 12 hours. Coatings deposited at both 350 °C and 500 °C had a thickness of 2.0±0.1 μm, as shown by the SEM images of the cross section of samples in Fig. 1.

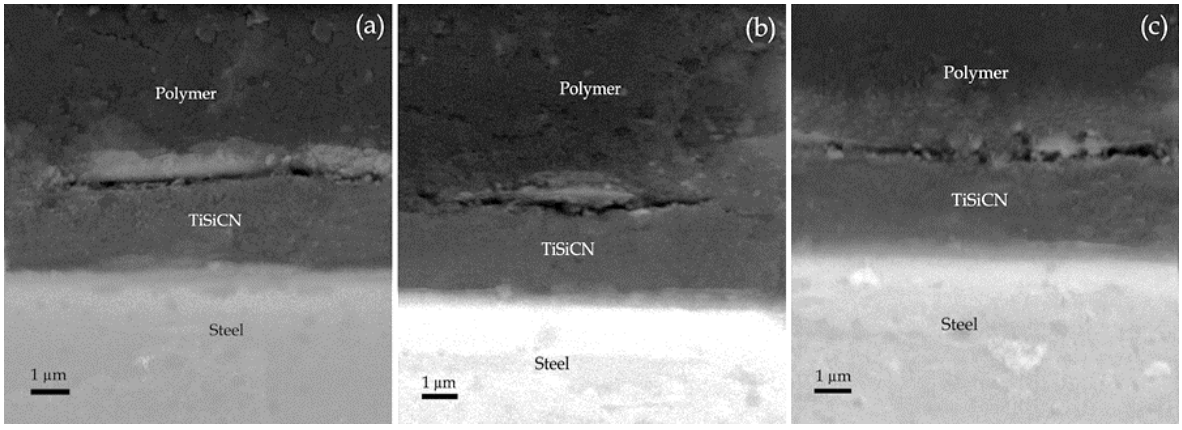

Fig. 1. Cross-section SEM images (backscattered electron mode) of TiSiCN coatings, (a) deposited at 350 °C, (b) deposited at 350 °C and annealed at 500 °C, (c) deposited at 500 °C.

Samples prepared at 350 °C were annealed in Ar atmosphere (10 Torr) at 500 °C for 3 hours, to investigate the effects of subsequent annealing treatment on the microstructure and mechanical properties of the coatings. After either deposition or annealing, specimens were cooled in the furnace under Ar atmosphere at the pressure of 10 Torr. Irrespective of the deposition temperature, as-deposited coatings showed a dark blue color, which did not change after possible annealing at 500 °C.

2.2. Characterization

The elemental composition of the coatings was determined by energy dispersive X-ray spectroscopy (EDS). The microstructure and phase structure of the coatings were investigated by High-Resolution Transmission Electron Microscopy (HR-TEM), using a Philips CM200 instrument operated at 200 kV, and by Glancing Incidence X-ray Diffraction (GI-XRD, with CuKα1 radiation, λ=0.154 nm, and grazing angle of 1°), using an 1830 PW Philips X-ray generator equipped with a PW 3020 Philips goniometer and a PW 3710 Philips control unit. The average crystallite size of the TiCN phase was assessed from the broadening of (200) diffraction peaks by the Scherrer equation. Fourier Transmission Infra-Red (FT-IR) spectroscopy in attenuated total reflection mode was used to investigate the surface chemistry and chemical bonding of the coating material, using a FTIR spectrometer PerkinElmer Spectrum System. The structure of free carbon was analyzed by Raman spectroscopy with a 532 nm laser excitation source, using a Raman spectrometer Takram P50C0R10. The thermal behavior of coatings was characterized by differential scanning calorimetry (DSC) and thermal gravimetric analysis (TGA) under Ar atmosphere in the temperature range of 200-1000 °C, using a TGA-DSC system TA Instruments, SDT Q600. In order to separate the coating material from the substrate, specimens were immersed in 12 M HCl solution. The coating fragments

were separated by filtration, then thoroughly rinsed with distilled water and acetone. The powder was dried at 80 °C in a vacuum oven, and 5 mg of the completely dried powder was used to perform the analysis. Hardness and elastic module were measured by a CSM Nano/Micro-Hardness Tester equipped with a Berkovich diamond indenter tip under a peak load of 50 mN (penetration depth < 250 nm). The reported hardness values of each specimen correspond to the average of five different measurements. Microscratch testing was performed to investigate the coating adhesion to the substrate, using a CSM Micro Scratch Tester, with a Rockwell C diamond tip (120° cone angle and tip curvature radius of 10 μm), with a load rate of 1 N/mm and tip horizontal speed of 50 mm/min. The scratch test was repeated three times for each sample to obtain an average value of the specimen critical load of failure. The latter was taken as an indication of coating adhesion since failure during microscratch testing occurred by film micro-cracking and chipping / spalling, as revealed by evidence not reported here, namely SEM observation of the scratches and acoustic emission output during scratching. Wear resistance was assessed by a pin-on-disc apparatus under a load of 500 gr at a sliding speed of 15 m/s. The pin was a 4 mm thick hardened AISI 52100 (64 HRC) ball with tip radius curvature of 10 mm.

3. Results

3.1. Elemental analysis

The results of elemental analysis performed by EDS, summarized in Table 1, show that with raising the deposition temperature there are relatively small changes in the coating composition, namely a significant reduction of the chlorine content and increase of the oxygen content. Chlorine impurities are obviously originated from Ti and Si precursors ($TiCl_4$ and $SiCl_4$), while the change of the oxygen impurity in the coatings is likely related to a relative increase of oxidant partial pressure due to enhancement of outgassing from reactor walls at higher

temperature. On the other hand, the increase of the oxygen content upon annealing, and the attendant decrease of chlorine impurity, is likely due to slight oxidation caused by the presence of oxygenated species in the annealing furnace atmosphere. The presence of iron is related to the steel substrate.

Table 1. Elemental composition (at. %) of TiSiCN coatings prepared at 500 °C or 350 °C, the latter also after annealing at 500 °C.

Annealing Temperature (°C)	**Deposition Temperature (°C)**	**Ti**	**Si**	**C**	**N**	**O**	**Cl**	**Fe**
-	350	31.8	13.2	23.8	25.3	1.7	2.1	2.1
500	350	31.7	13.0	23.2	25.1	3.8	1.3	1.9
-	500	34.1	13.5	22.2	22.9	4.6	1.0	1.7

Films grown by PECVD are notoriously prone to incorporate hydrogen to a variable extent depending on precursor gases, reducing environment and processing conditions. The hydrogen can be chemically bonded, chemisorbed on inner surfaces or trapped into the film [16]. In the present work, we could detect a significant content of hydrogen, up to about 5 at%, in coatings deposited at 350 °C, whilst, upon annealing at 500 °C, the hydrogen content in the film dropped to value below the detection limit (analysis performed by Glow Discharge Optical Emission Spectroscopy and not reported here). Similarly, the hydrogen content was below the detection limit in films grown at 500°C. In fact, the release and loss of hydrogen from TiSiCN coatings upon exposure to high temperature agrees with the reported thermal lability of Si-H and C-H bonds, e.g. in Si-doped a-C:H films [17], and of Si-N bonds in a-SiN_x:H films [18].

3.2. Microstructure analysis

XRD patterns of TiSiCN coatings prepared under different conditions, see Fig. 2, show, in addition to the reflections of the steel substrate, only diffraction peaks that can be attributed to TiCN phases. Therefore, due to the absence of the relevant diffraction peaks, silicon compounds

must be present in an amorphous state. In the XRD pattern of coatings deposited at 350 °C, broad TiCN peaks with relatively low preferential orientations are observed, implying the formation of small crystals of TiCN phases. Details of TiCN (200) peaks in the XRD pattern of TiSiCN coatings are indicated in Table 2. Either by post-deposition annealing at 500 °C or by increasing the deposition temperature to 500 °C, the peaks shift toward higher 2θ values and become sharper. These modifications in the pattern are associated with a decrease in the carbon content of TiCN crystals, as inferred from the shift of the peaks, and an increase in crystallinity, as obviously shown by the increased diffracted intensity and by the increase of the average crystallite size determined from the broadening of the TiCN (200) peak. Both these effects are stronger for coatings deposited at 500 °C compared to those deposited at 350 °C and annealed at 500 °C.

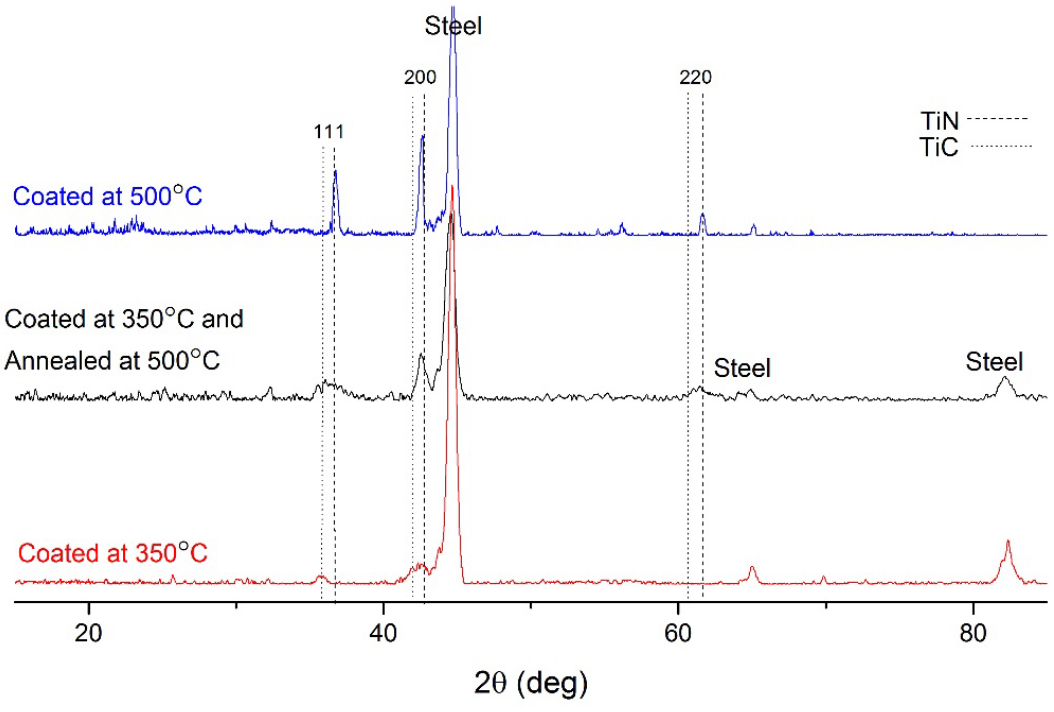

Fig. 2. XRD patterns of TiSiCN coatings grown at 500 °C and 350 °C, the latter also after annealing at 500 °C, as indicated.

Table 2. Diffraction angle of TiCN (200) peaks and crystallite size derived from peak broadening by the Scherrer equation for TiSiCN coatings prepared under given conditions.

Deposition Temperature (°C)	**Annealing Temperature (°C)**	**2θ (°)**	**Crystallite size (nm)**
350	-	42.3	6.3
350	500	42.5	12
500	-	42.6	21

For detailed investigation of the coatings microstructure, samples were analyzed by HR-TEM. Fig. 3 shows TEM micrographs of the different TiSiCN coatings with selected area electron diffraction (SAED) patterns in the insets; HR-TEM images of the same samples are presented in Fig. 4. In the case of coatings grown at 350 °C (Fig. 3-a), the micrograph reveals a spotted appearance, with a faint contrast between dark spots and the surrounding area, suggesting a relative enrichment in titanium in the former compared to the latter. The SAED pattern in the inset of Fig. 3-a does not show any evidence of the presence of crystalline phases, confirming the dominant amorphous nature of the coating material as revealed by the XRD pattern in Fig. 2. In fact, HR-TEM imaging of the dark spots (Fig. 4-a) reveals the presence of small areas of low crystalline order surrounded by the fully amorphous matrix. For the sample deposited at 350 °C and annealed at 500 °C, continuous diffuse rings appear in the SAED pattern (inset of Fig. 3-b) which can be indexed as the face centered cubic (FCC) TiCN crystalline phase, in agreement with the XRD results. Expectedly, annealing produces a more developed microstructure compared to the as-deposited coating material at 350 °C. This is made evident by the stronger contrast, in Fig. 3-b compared to Fig. 3-a, between bright area and dark spots, which, as already noted above, probably correspond to predominantly amorphous (bright) and nanocrystalline (dark) regions and, therefore, are associated with local enrichment in either silicon or titanium, respectively. HR-TEM images of the bright and dark areas are shown in Fig.4-b and Fig.4-c, respectively. In either case, the analysis reveals a nanosized microstructure consisting of TiCN nanocrystals surrounded by an amorphous matrix, similarly to the as-

deposited coating (Fig. 4-a). However, in the bright area, see Fig. 4-c, smaller TiCN nanocrystals with enhanced number density can be seen, while the dark area is characterized by the presence of larger nanocrystals and, overall, a higher degree of crystallization.

The TEM image of the film deposited at 500 °C, in Fig. 3-c, shows a seemingly nanocrystalline and well developed microstructure, due to the formation of large TiCN crystals, with size ranging from about 20 to over 50 nm, as previously inferred from the XRD pattern in Fig. 2 and now confirmed by the presence of relatively sharp rings in the SAED pattern of the inset of Fig. 3-c, which can be obviously indexed as the FCC TiCN phase. The HR-TEM micrographs in Fig. 4-d reveal finer details of the microstructure, namely the nanocomposite nature of the coating, consisting of relatively large crystals, compared to those observed in coatings deposited at 350 °C and annealed at 500 °C, enveloped by an amorphous sheath.

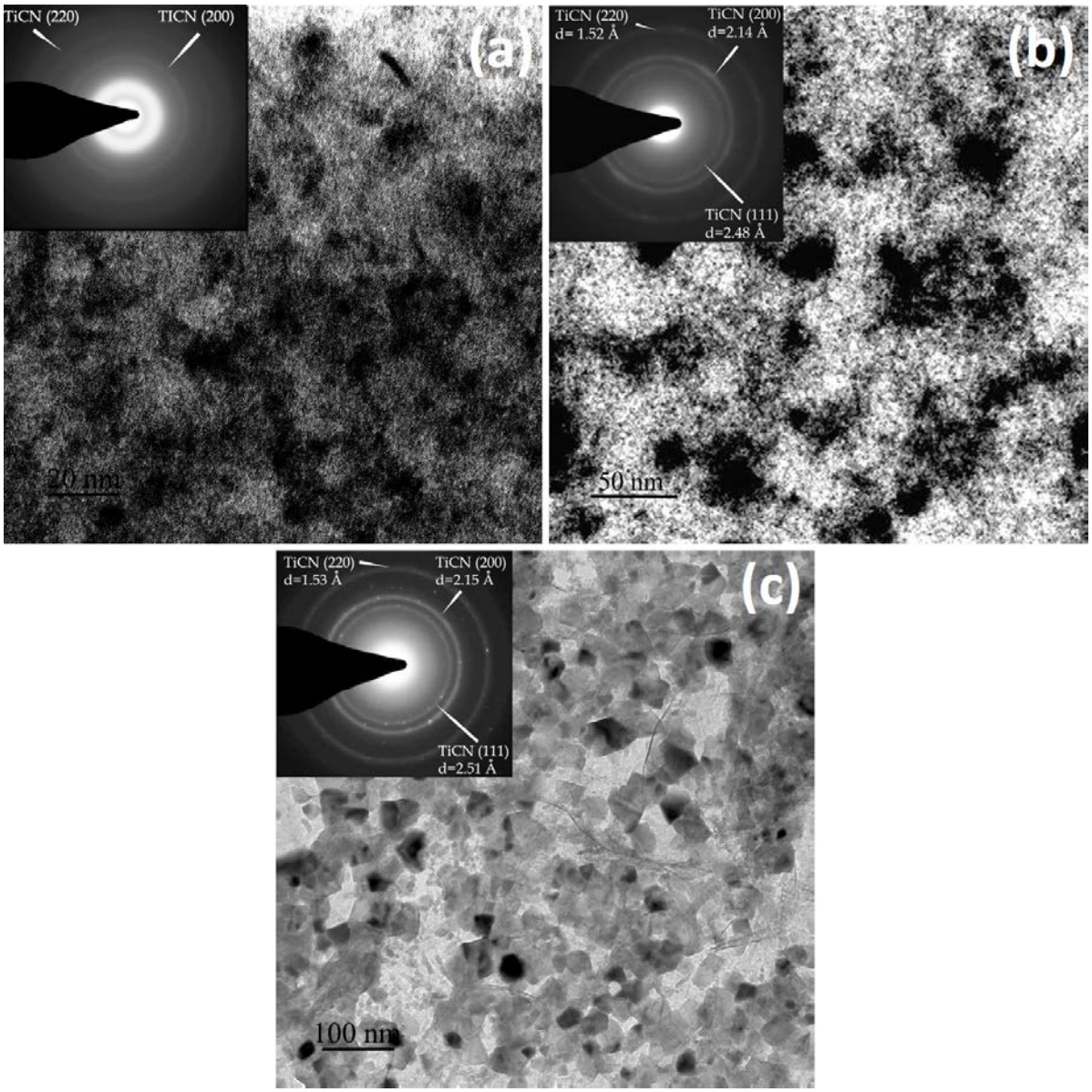

Fig. 3. TEM micrographs and corresponding SAED patterns in the insets, of TiSiCN coatings, (a) deposited at 350 °C, (b) deposited at 350 °C and annealed at 500 °C, (c) deposited at 500 °C.

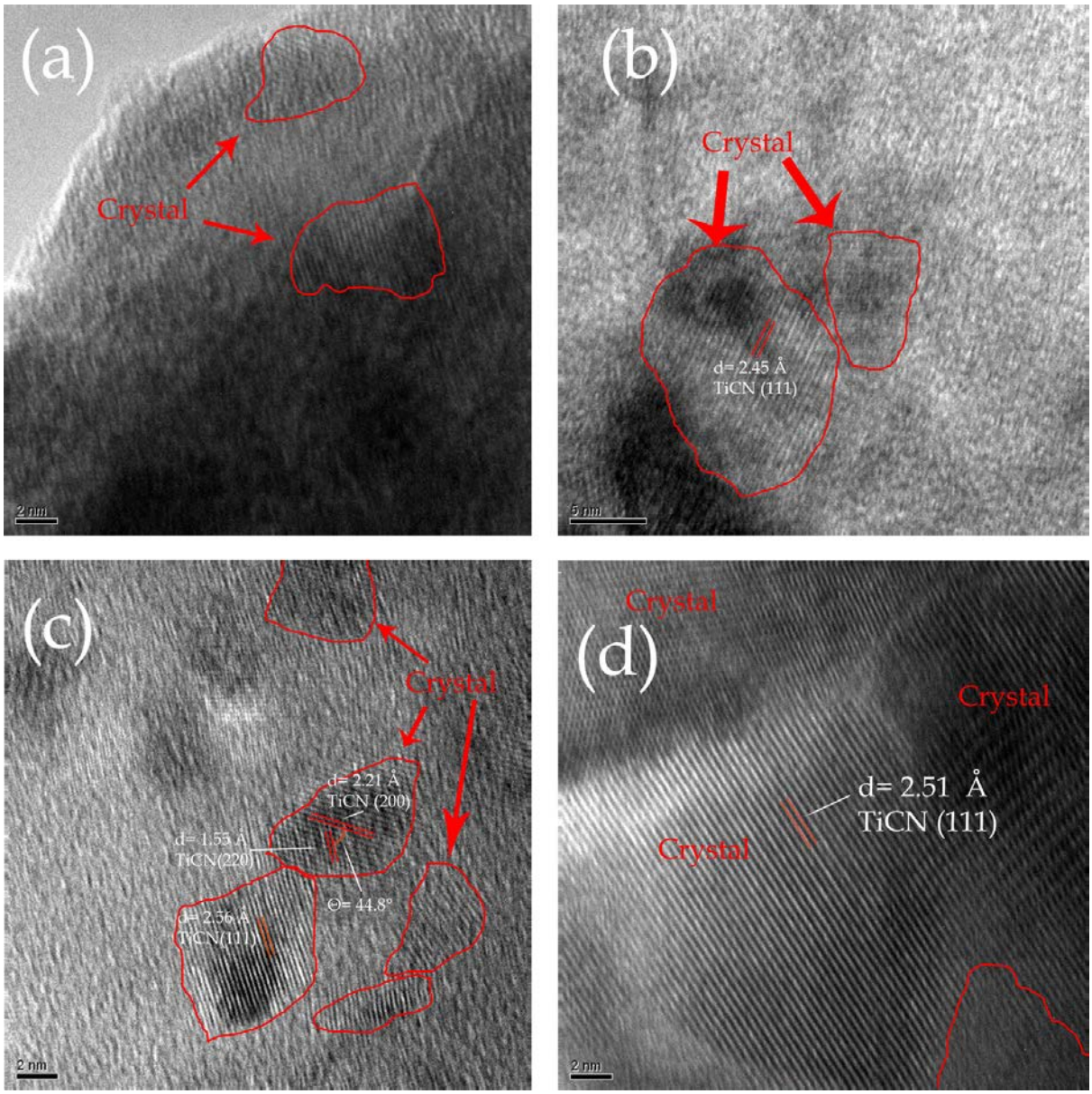

Fig. 4. HR-TEM micrographs of (a) TiSiCN coatings deposited at 350 °C; (b) bright area and (c) dark spot region of Fig. 3-b in the coating deposited at 350 °C and annealed at 500 °C, (d) TiSiCN coating deposited at 500 °C.

The results of DSC and TGA analysis for the TiSiCN coating deposited at 350 °C are shown in Fig. 5. Two broad exothermic peaks appear in the DSC thermogram, with onset temperature of about 300 °C and 700 °C, which –in the light of the evidence provided by XRD and TEM examination– can be related to nanocrystal segregation and recovery phenomena. Namely, we can argue that the first exothermic peak corresponds to the decomposition of the supersaturated solid solution, formed at the low growth temperature of 350 °C, into the nanocrystalline TiCN

phase and the amorphous Si rich and carbon phases (see further on), while the exothermic reaction observed above 700 °C is probably related to rearrangement or elimination of lattice defects and possibly coarsening of TiCN crystals [19]. The weight loss observed in the TGA curve of Fig. 5 is likely due to the release of small hydrocarbons and chlorine from the coatings. Possible release of chlorine agrees with the results of the elemental analysis of the coatings, showing a significant drop of its content in coatings deposited at 500 °C (Table 1).

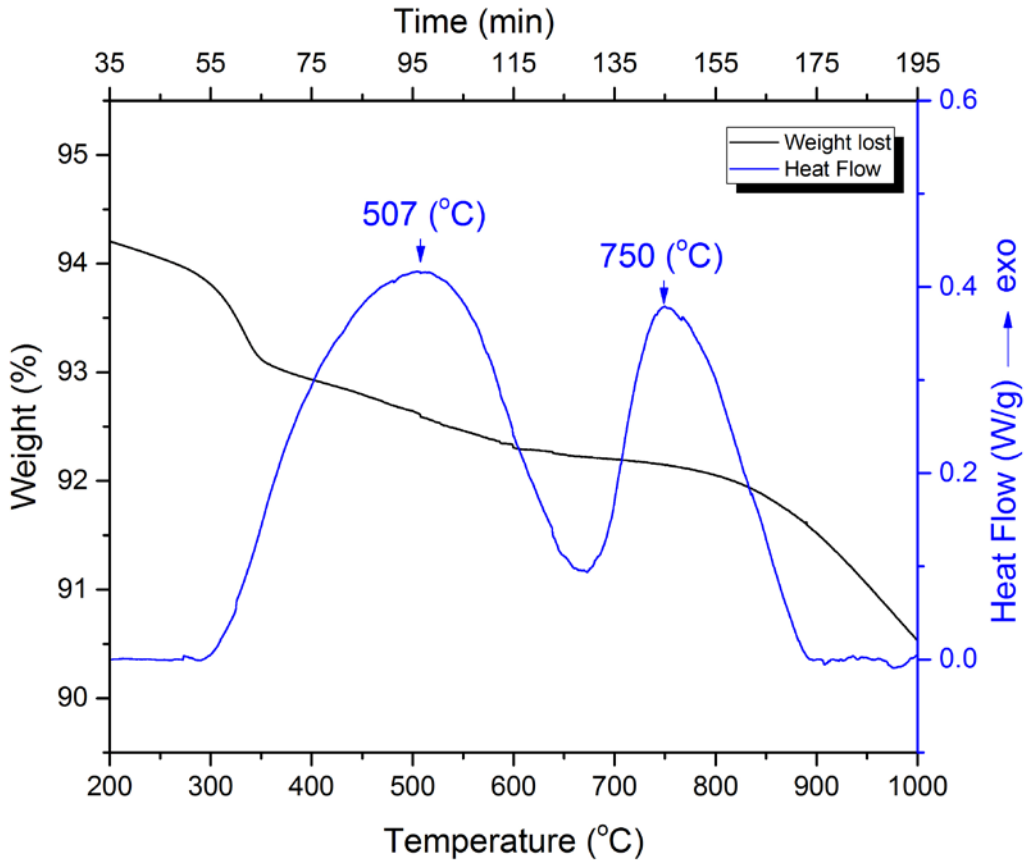

Fig. 5. Variation of weight and heat flow as a function of temperature for a TiSiCN coating deposited at 350 °C.

As previously mentioned, XRD patterns exhibit only peaks related to TiCN phase indicating that silicon compounds must be amorphous. Therefore, we performed FT-IR analysis of the coatings to gather evidence about the chemical bonding of silicon in the amorphous phase. In the FTIR spectra of Fig. 6, the band at 798 cm^{-1} and the band at 946 cm^{-1} can be assigned to Si-

C [20, 21] and Si-N [22] bonds, respectively. In the wavenumber range 1000-1200 cm^{-1} different vibrational features strongly overlap, with the more intense peak corresponding to the overlapping of Ti-O-Si (at 1040 cm^{-1}) and Si-N-Si (at 1100 cm^{-1}) bands and the peak shoulder on the higher wavenumber side corresponding to Si-O-Si (~1200 cm^{-1}), following the band assignment given in [23]. By raising the deposition temperature to 500 °C or by subsequent annealing at the same temperature, FTIR spectra reveal an increase in the peak intensity of C=C, C=N (1580-1630 cm^{-1}) [24] and C-O (1420 cm^{-1}) [25], which is associated with an increasing content of amorphous carbon phase within the structure. For the specimen coated at 350 °C, the C-H_n (2921 cm^{-1}) [25] peak is also observed, at variance with the spectra recorded for the specimens coated at 350 °C and annealed at 500 °C. The presence of the C-H_n peak in the FTIR spectra of sample grown at 350 °C confirms possible release of hydrocarbon compounds from these films during TGA measurements.

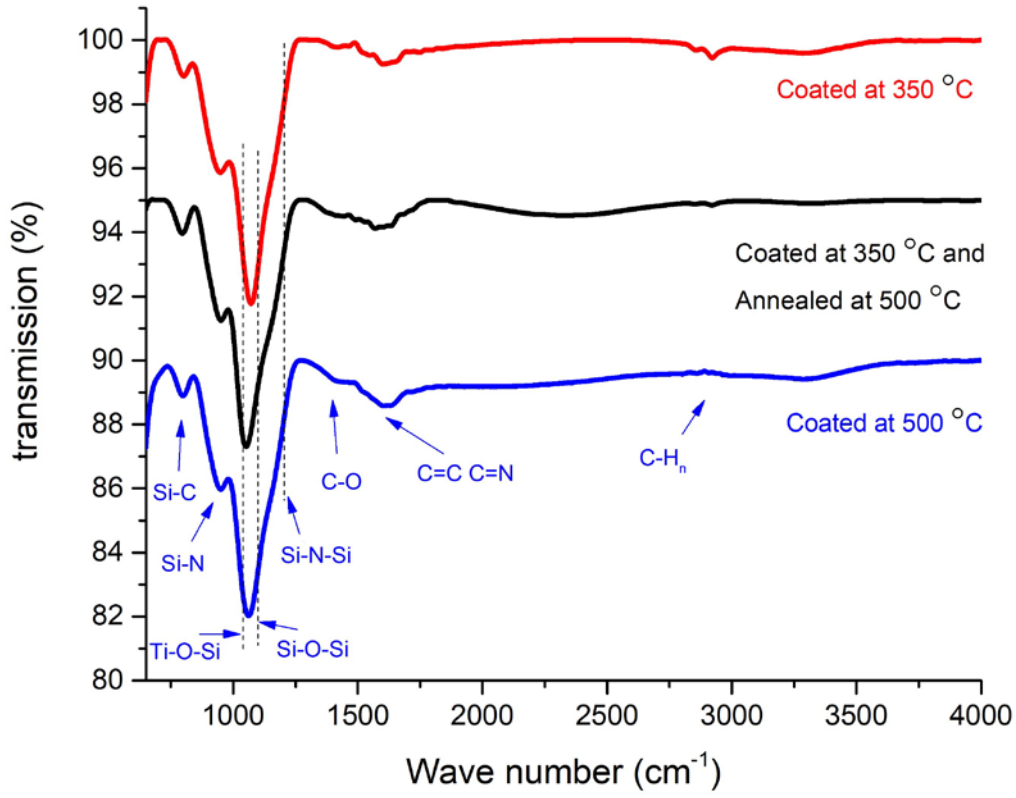

Fig. 6. FT-IR spectra of TiSiCN coatings deposited at 350 °C or 500 °C and at 350 °C with subsequent annealing at 500 °C, as indicated.

Further evidence concerning the chemical state of carbon in the coating was sought for by performing Raman spectroscopy analysis of the samples, as shown by the graph of Fig. 7. The peaks corresponding to the D (about 1300 cm^{-1}) and G (about 1600 cm^{-1}) bands [26] in the Raman spectra of TiSiCN films obviously reveal the presence of carbon in the coatings. In addition, the peaks in the range of 200-700 cm^{-1} are caused by scattering in acoustic and optical modes due to the presence of TiCN crystals with FCC lattice [27, 28]. As revealed by the spectra in Fig. 7, the most evident change between the sample coated at 350 °C and the sample grown at the same temperature and annealed at 500 °C, is the increased intensity of the TiCN bands in the low wave number region of the spectrum, which is an indication of a relative increase in the amount of the phase and of its higher degree of crystallinity. A further change in the Raman spectra brought about by annealing is the reduction of the intensity ratio of the D band to the G band, I(D)/I(G), which is also a possible indication of a relative improvement in the degree of crystallinity of the carbon phase. On the other hand, by comparing the Raman spectrum of the coating deposited at 500 °C and the Raman spectrum of the coating deposited at 350 °C and annealed at 500 °C, a higher value of the I(D)/I(G) intensity ratio is apparent for the former. Notably the I(D)/I(G) intensity ratio for the coating deposited at 500 °C is also slightly higher than that for the coating deposited at 350 °C. Therefore, the lower I(D)/I(G) value for the latter sample cannot be associated with a relative change in the amount of amorphous and graphitic carbon (in fact, at lower temperature we would expect it to be higher). Then, the increase of I(D)/I(G) ratio in the coating deposited at 500 °C may be tentatively ascribed to the formation of larger carbon clusters in the latter coatings compared to those deposited at 350 °C and in case annealed at 500 °C.

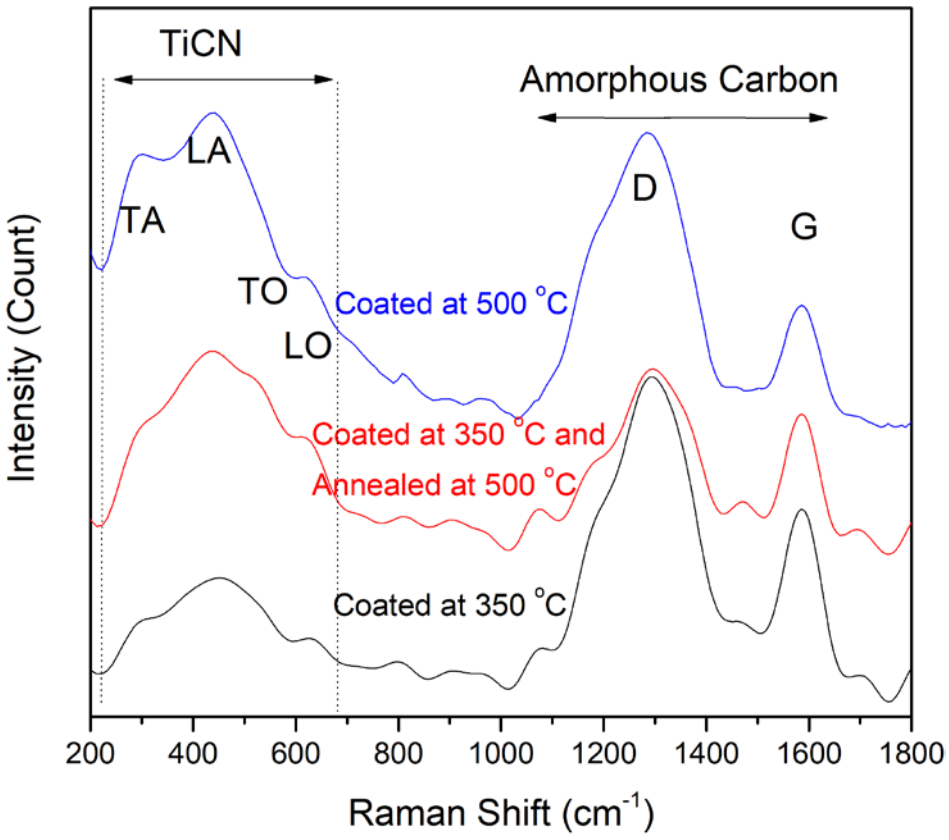

Fig. 7. Raman spectra of TiSiCN coatings deposited at 500 °C and at 350 °C, the latter with and without annealing at 500 °C.

3.3. Mechanical properties of TiSiCN coatings

In the present paragraph, we provide an overview of the mechanical properties of TiSiCN coatings, reporting results of indentation, scratch and wear testing, while leaving to future work a more in-depth investigation of the mechanical behavior and the wear mechanism of the coatings. We show in Table 3 the indentation hardness, the elastic modulus and the critical load of failure L_C for TiSiCN coatings deposited at 350 °C –with and without subsequent annealing at 500 °C– and at 500 °C. The lowest values of hardness, elastic modulus and critical load of failure were measured for the coating deposited at 350 °C. On the other hand, the TiSiCN coating deposited at 350 °C and annealed at 500 °C showed the highest hardness and adhesion, compared to either samples deposited at 350 °C or 500 °C.

Table 3. Indentation hardness, elastic modulus and critical load of failure of TiSiCN coatings deposited at 350 °C, the same with subsequent annealing at 500 °C and at 500 °C.

Deposition temperature (°C)	Annealing temperature (°C)	Hardness (GPa)	Elastic module (GPa)	Critical load of failure (N)
350	-	28±2	321±16	2.2±0.2
350	500	42±3	338±20	3.5±0.2
500	-	39±3	341±22	3.1±0.1

Friction coefficients of TiSiCN coatings as a function of sliding distance and wear cycles are shown in Fig. 8. The initial friction coefficient of the coating deposited at 350 °C (after sliding distance of 200 m) was 0.3. Either by following annealing at 500 °C or by deposition at 500 °C, a lower (initial) friction coefficient was observed. In particular, the lowest value of the friction coefficient of 0.1 was measured for the specimen coated at 350 °C and subsequently annealed at 500 °C. In all coatings, a reduction of the friction coefficient was observed after a sliding distance of 100-300 m, which is likely due to the accumulation of carbon particles along the wear track. These particles act as solid lubricant, hence reducing the friction coefficient. Steel-steel friction coefficient is reported in the literature in the range of 0.6-0.7 [29]. Considering a friction coefficient of 0.6, the wear life (defined as the sliding distance required for complete removing of the coating) is measured as 450 m, for the sample coated at 350 °C, 1000 m, for the sample coated at 350 °C and annealed at 500 °C, and 850 m, for the sample coated at 500 °C.

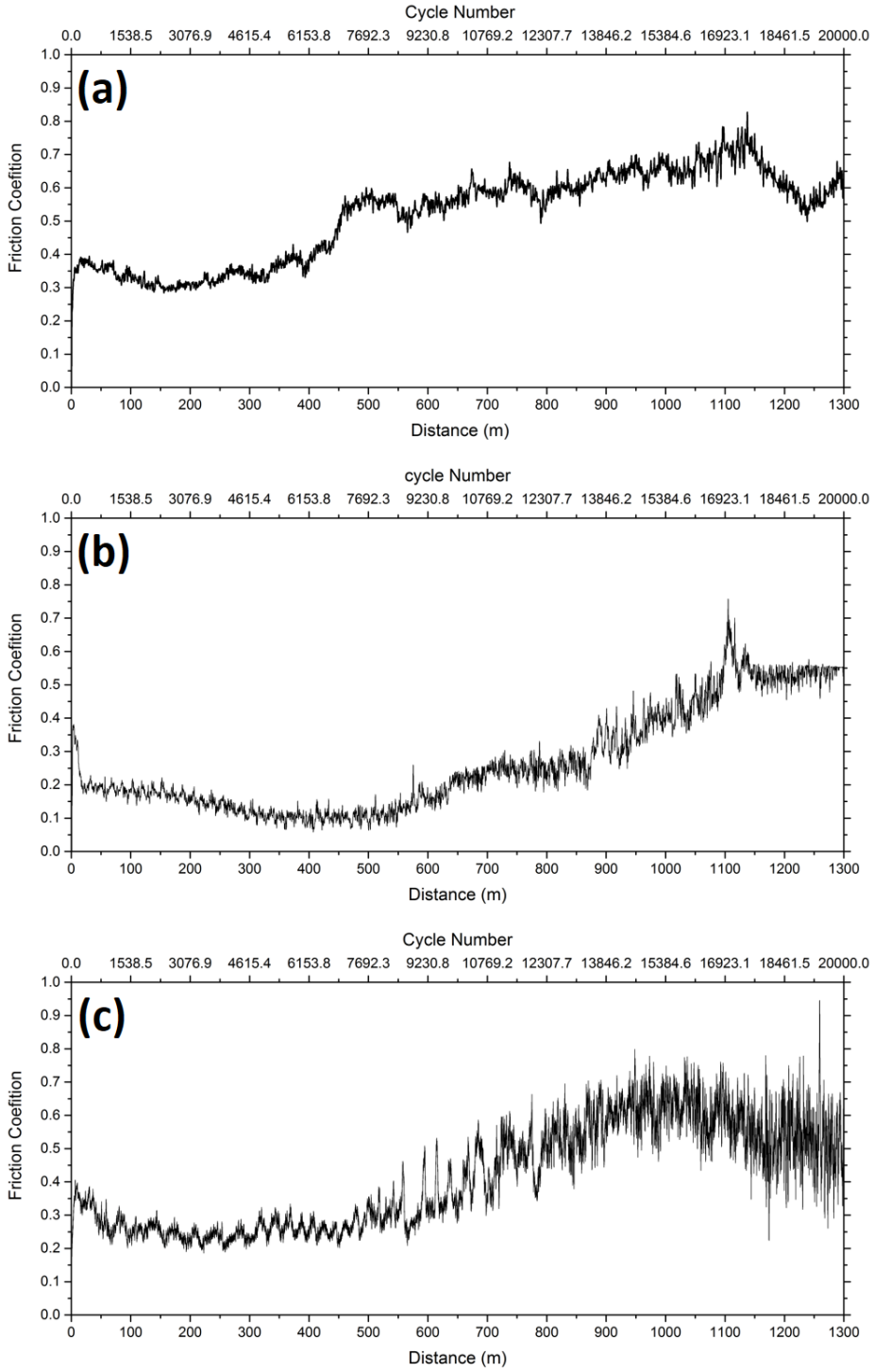

Fig. 8. Friction coefficient as a function of sliding distance and wear cycles for TiSiCN coatings (a) deposited at 350 °C, (b) deposited at 350 °C and annealed at 500 °C, (c) deposited at 500 °C.

Figure 9 shows the SEM images and cross sectional profiles of the wear tracks on the different coatings. The wear tracks on TiSiCN coatings, either deposited or annealed at 500 °C, are

uniform and smooth, in particular without sign of coating delamination. Besides, loose wear debris are absent at either side of the wear tracks suggesting high resistance to plastic deformation for these coatings. Conversely, more severe abrasion damage is apparent from the wear scar of the coating deposited at 350 °C, in Figure 9 (a), with some evidence of ploughing. The width of the wear track was measured as ~929 µm for the coating deposited at 350 °C; 453 µm for the coating deposited at 350°C and annealed at 500°C; and 482 µm for the coating deposited at 500 °C. From the wear track profile we calculated the worn volume and the wear rate $K_w = \frac{V}{FS}$, where V is the worn volume, S is the total sliding distance (m) and F is the applied load (N), obtaining the following values: 1.90×10^{-5} mm^3/Nm for the coating deposited at 350 °C; 6.68×10^{-6} mm^3/Nm for the coating deposited at 350 °C and annealed at 500 °C; and 7.98×10^{-6} mm^3/Nm, for the coating deposited at 500 °C.

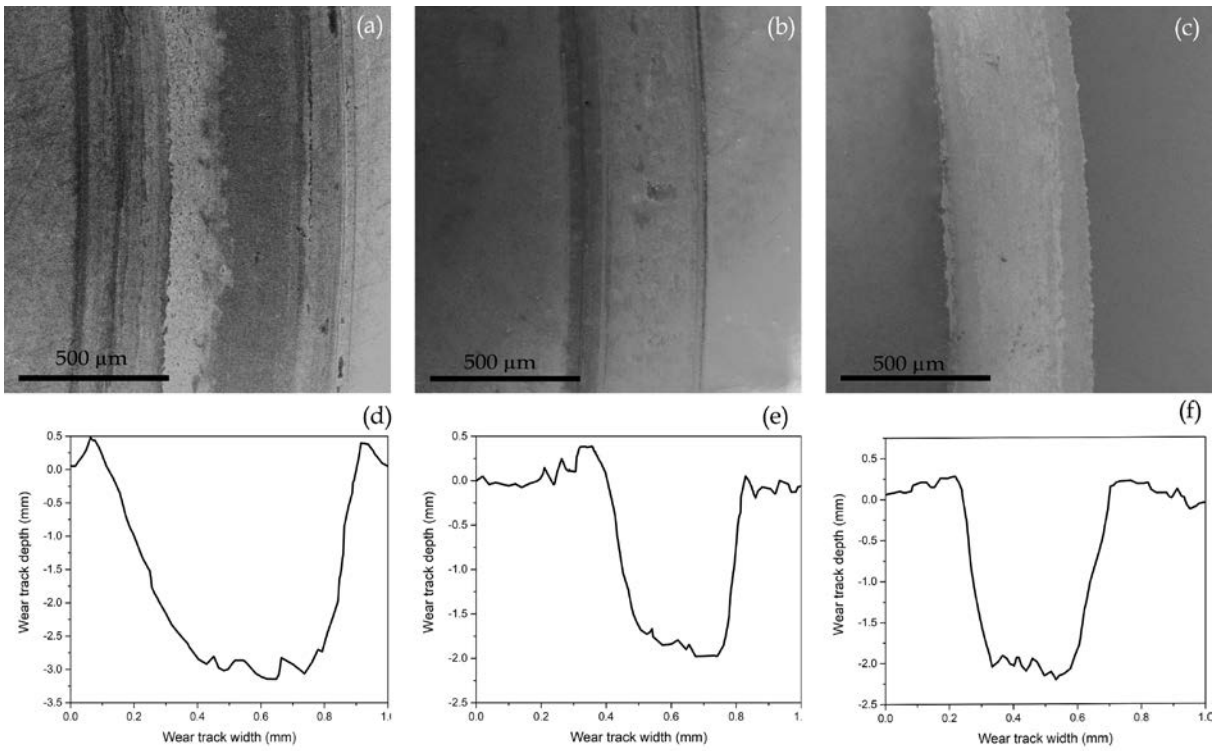

Fig. 9: SEM images and cross-sectional profiles of the wear tracks on TiSiCN coatings (a) and (d) deposited at 350 °C, (b) and (e) deposited at 350 °C and annealed at 500 °C and (c) and (f) deposited at 500 °C.

4. Discussion

The EDS results reveal that coatings deposited at either 350 °C, with or without annealing at 500 °C, or 500 °C have similar chemical composition, apart from the presence of a relatively high hydrogen content in the coatings deposited at 350 °C. However, according to XRD and TEM analysis, the structure of the coating deposited at 350 °C is mostly amorphous with a small fraction of nanosize TiCN crystals, which implies that only a comparatively small part of the overall titanium content contributed to the formation of TiCN crystals. In spinodal decomposition, though there is no need to provide activation energy, phase segregation requires diffusion. Hence, the temperature has a significant influence on the structure of the coating as it affects the diffusion rate [30]. For instance, diffusion of Si through a 5 nm distance away from the TiN grain boundaries requires about 50000 s at 300 °C [31]. It was also reported that at deposition temperature lower than 400 °C, TiN coatings deposited via PECVD using $TiCl_4$ precursor had an amorphous structure [32]. Similarly, in the present work, the low deposition temperature of 350 °C constrains the formation of TiCN crystals, with excess Ti forming a supersaturated solid solution. Since the diffusion distance of atoms at 350 °C is limited, only partial separation of silicon and titanium compounds occurs, leading to the formation of segregated regions. On the other hand, by raising the deposition temperature, the acceleration of surface and volume diffusion [33] allows for much faster phase separation processes and microstructure arrangement.

A schematic illustration of the microstructure of TiSiCN coatings formed under different conditions, and in particular as a result of post-deposition annealing, is shown in Fig. 10. Upon exposure to the annealing temperature of 500 °C, the supersaturated solid solution becomes unstable towards spinodal decomposition [13], triggering the formation of TiCN crystals, provided that a locally high concentration of titanium is available. The strong inhibition of the growth of TiCN crystals may be explained as a result of the local depletion of titanium and the

attendant precipitation of Si and C rich amorphous phases at the crystal growth front [8, 31], acting as a diffusion barrier. Therefore, the number density of TiCN nanocrystals in different regions is determined by the local content of titanium, with a relatively higher number density of smaller size crystals occurring in regions of relatively low titanium concentration. Due to the formation of TiCN nanocrystals from supersaturated solid solution during annealing, TiCN (200) peak broadening is observed in the XRD pattern. Structural evolution from supersaturated solid solution to nanocomposite structure, consisting of TiCN crystals and amorphous carbon particles separated by the SiCN amorphous matrix, gives rise to a broad peak at about 500 °C in the DSC diagram (Fig. 5).

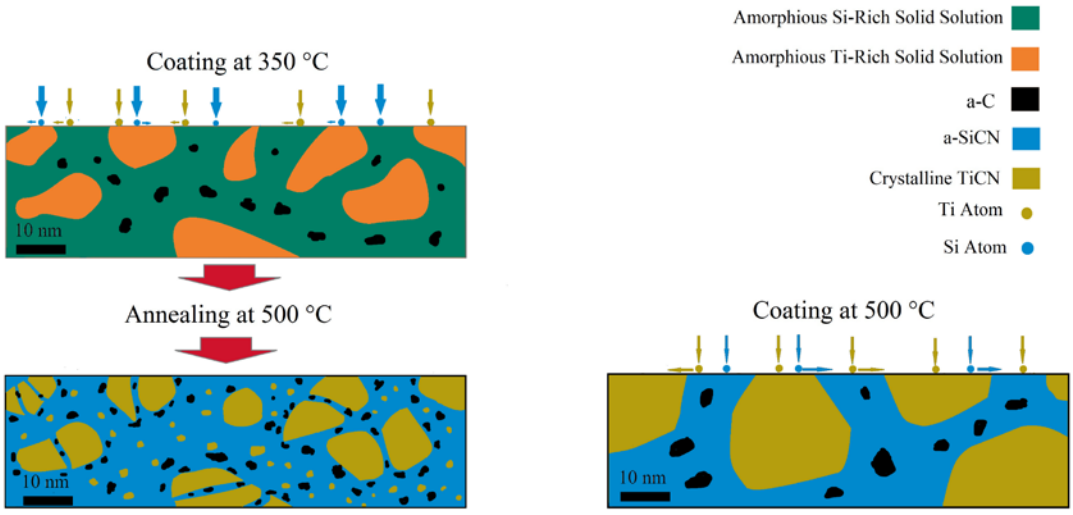

Fig. 10: Schematic of the microstructure of TiSiCN coatings deposited at 350 °C and 500 °C, and of the microstructural evolution of TiSiCN coating deposited at 350 °C after annealing at 500 °C.

Compared to the coating deposited at 350 °C and annealed at 500 °C, the coating prepared at 500 °C exhibits larger TiCN crystallite size. Although both coatings were exposed to 500 °C for an equal time interval, considerable difference in crystallite size is observed, pointing to a fundamental difference in the kinetic processes controlling the formation of the coating microstructure, namely surface diffusion –during deposition at 500 °C– and lattice or grain boundary diffusion –during annealing at 500 °C following deposition at 350 °C. In other words,

the slower rate of bulk diffusion compared to surface diffusion [34] can be the main reason for smaller TiCN crystals in the coating deposited at 350 °C and annealed at 500 °C.

FT-IR results suggest that the temperature of deposition or annealing has no significant effect on peak intensity ratio of Si-C, Si-N, Si-N-Si and Si-O-Si bonds. In other words, the temperature does not appear to have a significant influence on the formation and composition of silicon compounds. Even increasing the oxygen content (as a result of raising the deposition/annealing temperature, see Table 1) has no effect on this ratio, suggesting that possible oxygen impurities are absorbed by the titanium rich phase. According to FT-IR and Raman spectroscopy results, the relative amount of C-C bond increases at higher temperature, suggesting the formation of larger and or less defective amorphous carbon domains. In this respect, it is worth noticing that the amount of Si-C bonds remains constant, irrespective of the deposition conditions, while, according to the XRD analysis, there may be a reduction of the carbon content in the TiCN phase, with raising deposition temperature. Therefore, it is possible to postulate that the extraction of carbon from TiCN phase is the main reason for the higher content of the amorphous carbon phase (in fact, even though amorphous carbon was not observed in TEM micrographs, the results of both FT-IR and Raman spectroscopy confirm the presence of this phase in the films). As a further remark, we observe that smaller size carbon clusters are probably formed in the coatings grown at 350 °C and annealed at 500 °C, compared to coatings grown at 500 °C. In fact, as already noted above, the results of Raman spectroscopy are suggestive of sensible changes of the carbon phase, which may be amenable to the above interpretation. In addition, the presence of smaller carbon particles in the annealed sample is a straightforward explanation for the observed lower value of the friction coefficient.

Summing up the above comments, coatings deposited at 350 °C mainly consist of amorphous phases and a low fraction of a crystalline phase. The prevailing amorphous nature of these coatings, and possibly the residual hydrogen content, is the reason for their much lower

hardness compared to coatings processed at higher temperature. Upon annealing at 500 °C, the structure evolves under strong time and space constraints forming a fine nanocomposite structure leading to a significant increase of the hardness. Higher content of free carbon and/or the refinement of amorphous carbon particles in coatings deposited at 350 °C and annealed at 500 °C improves the self-lubrication capability of the material, providing lower values of friction coefficient compared to the coatings deposited at 350 °C. Obviously, annealed coatings show an improved wear behavior, due to the higher hardness and the lower friction coefficient.

5. Conclusions

Super hard (34-46 GPa) quaternary TiSiCN coatings deposited at 350 °C, with or without subsequent annealing at 500 °C, and at 500 °C showed a nanocomposite structure consisting of TiCN crystals and amorphous carbon in an amorphous SiCN matrix. At the low deposition temperature of 350 °C, due to the slow diffusion rate, titanium mostly remains in the supersaturated solid solution of the amorphous SiCN matrix, forming only a small amount of crystalline phase. Annealing at 500 °C of the coatings deposited at 350 °C leads to the formation of a fine nanocrystalline TiCN phase, which translates into a distinct improvement of the mechanical properties of the coatings. In addition, since the carbon content in the TiCN structure is reduced by annealing at 500 °C, the relative increase in the phase fraction of amorphous carbon results in the lowering of the friction coefficient down to about 0.1. The smallest grain size (about 12 nm from XRD peak broadening, and even less according to TEM observation) was observed for the annealed coating compared to coatings deposited at 500 °C (with crystal size in the range from about 20 nm to over 50 nm). Overall, annealed coatings showed better characteristics, such as higher hardness, adhesion and wear resistance, compared to coatings deposited at 500 °C, apparently as a result of the improved control over the formation of the microstructure achieved by post deposition annealing. Accordingly, the present

study reveals that the preparation of TiSiCN coatings by deposition at lower temperature (350 °C) followed by annealing at higher temperature (500 °C) yields smaller grain size and improves wear and tribological properties compared to coatings deposited at the higher temperature without further annealing.

References

[1] H.C. Barshilia, B. Deepthi, K. Rajam, Transition metal nitride-based nanolayered multilayer coatings and nanocomposite coatings as novel superhard materials, in: S. Zhang (Ed.), Nanostructured Thin Films and Coatings. Mechanical Properties, first ed., CRC Press, Boca Raton, 2010, pp. 427-480.
[2] J. Musil, Hard nanocomposite coatings: thermal stability, oxidation resistance and toughness, Surf. Coat. Tech. 207 (2012) 50-65.
[3] Y. Cheng, T. Browne, B. Heckerman, E. Meletis, Mechanical and tribological properties of nanocomposite TiSiN coatings, Surf. Coat. Tech. 204 (2010) 2123-2129.
[4] D. Ma, S. Ma, K. Xu, Influence of Si content on Nano-structured Ti–Si–N films coated by pulsed-dc plasma enhanced CVD, Surf. Coat. Tech. 184 (2004) 182-187.
[5] F. Movassagh-Alanagh, A. Abdollah-zadeh, M. Aliofkhazraei, M. Abedi, Improving the wear and corrosion resistance of Ti–6Al–4V alloy by deposition of TiSiN nanocomposite coating with pulsed-DC PACVD, Wear, 390 (2017) 93-103.
[6] S. Abraham, E.Y. Choi, N. Kang, K.H. Kim, Microstructure and mechanical properties of Ti-Si-CN films synthesized by plasma-enhanced chemical vapor deposition, Surf. Coat. Tech. 202 (2007) 915-919.
[7] I. Endler, M. Höhn, J. Schmidt, S. Scholz, M. Herrmann, M. Knaut, Ternary and quarternary TiSiN and TiSiCN nanocomposite coatings obtained by Chemical Vapor Deposition, Surf. Coat. Tech. 215 (2013) 133-140.
[8] S. Ma, D. Ma, Y. Guo, B. Xu, G. Wu, K. Xu, P.K. Chu, Synthesis and characterization of super hard, self-lubricating Ti–Si–C–N nanocomposite coatings, Acta Mater. 55 (2007) 6350-6355.
[9] Y. Guo, S. Ma, K. Xu, T. Bell, X. Li, H. Dong, On the oxidation resistance of superhard Ti–Si–C–N coatings, J. Mater. Res. 23 (2008) 2420-2428.
[10] A.A. El-Rahman, R. Wei, Effect of ion bombardment on structural, mechanical, erosion and corrosion properties of Ti–Si–C–N nanocomposite coatings, Surf. Coat. Tech. 258 (2014) 320-328.
[11] J. Lin, R. Wei, D.C. Bitsis, P.M. Lee, Development and evaluation of low friction TiSiCN nanocomposite coatings for piston ring applications, Surf. Coat. Tech. 298 (2016) 121-131.
[12] S. Vepřek, S. Reiprich, A concept for the design of novel superhard coatings, Thin Solid Films, 268 (1995) 64-71.
[13] S. Veprek, M.G. Veprek-Heijman, P. Karvankova, J. Prochazka, Different approaches to superhard coatings and nanocomposites, Thin Solid Films, 476 (2005) 1-29.
[14] S. Veprek, H.-D. Männling, M. Jilek, P. Holubar, Avoiding the high-temperature decomposition and softening of ($Al_{1-x}Ti_x$) N coatings by the formation of stable superhard nc-($Al_{1-x}Ti_x$)N/a-Si_3N_4 nanocomposite, Mat. Sci. Eng. A, 366 (2004) 202-205.
[15] T. Cholakova, V. Chitanov, D. Chaliampalias, L. Kolaklieva, R. Kakanakov, C. Bahchedjiev, N. Petkov, C. Pashinski, G. Vourlias, N. Vouroutzis, Study of the structural and

mechanical properties of nanocrystalline TiAlSiN gradient coatings, J. Nano Res. 27 (2014) 15-24.
[16] L. Martinu, O. Zabeida, J. Klemberg-Sapieha, Plasma-enhanced chemical vapor deposition of functional coatings, in: Handbook of Deposition Technologies for Films and Coatings, third ed., Elsevier, (2010), pp. 392-465.
[17] W.-J. Wu, M.-H. Hon, Thermal stability of diamond-like carbon films with added silicon, Surf. Coat. Tech. 111 (1999) 134-140.
[18] C. Ling, C. Kwok, K. Prasad, Relative Hydrogen Content in Plasma-Enhanced CVD Silicon Nitride Films: Substrate Temperature Dependence and Effect of Thermal Annealing, Phys. Status. Solidi A, 89 (1985) 39-43.
[19] A.A. Voevodin, D.V. Shtansky, E.A. Levashov, J.J. Moore, Nanostructured thin films and nanodispersion strengthened coatings, Springer Science & Business Media, New york, (2006).
[20] Q. Cheng, S. Xu, K.K. Ostrikov, Single-step, rapid low-temperature synthesis of Si quantum dots embedded in an amorphous SiC matrix in high-density reactive plasmas, Acta Mater. 58 (2010) 560-569.
[21] C. Vix-Guterl, I. Alix, P. Ehrburger, Synthesis of tubular silicon carbide (SiC) from a carbon–silica material by using a reactive replica technique: mechanism of formation of SiC, Acta Mater. 52 (2004) 1639-1651.
[22] E. Vassallo, A. Cremona, F. Ghezzi, F. Dellera, L. Laguardia, G. Ambrosone, U. Coscia, Structural and optical properties of amorphous hydrogenated silicon carbonitride films produced by PECVD, App. Surf. Sci. 252 (2006) 7993-8000.
[23] F. Rose, B. Marchon, V. Rawat, D. Pocker, Q.-F. Xiao, T. Iwasaki, Ultrathin TiSiN overcoat protection layer for magnetic media, J. Vac. Sci. Tech. A, 29 (2011) 051502.
[24] C. Oliveira, L. Gonçalves, B. Almeida, C. Tavares, S. Carvalho, F. Vaz, R. Escobar_Galindo, M. Henriques, M. Susano, R. Oliveira, XRD and FTIR analysis of Ti–Si–C–ON coatings for biomedical applications, Surf. Coat. Tech. 203 (2008) 490-494.
[25] S. Sedira, S. Achour, A. Avci, V. Eskizeybek, Physical deposition of carbon doped titanium nitride film by DC magnetron sputtering for metallic implant coating use, App. Surf. Sci. 295 (2014) 81-85.
[26] J. Robertson, Diamond-like amorphous carbon, Mat. Sci. Eng. R, 37 (2002) 129-281.
[27] I. Dreiling, A. Haug, H. Holzschuh, T. Chassé, Raman spectroscopy as a tool to study cubic Ti–C–N CVD coatings, Surf. Coat. Tech. 204 (2009) 1008-1012.
[28] K. Kuptsov, P.V. Kiryukhantsev-Korneev, A. Sheveyko, D. Shtansky, Structural transformations in TiAlSiCN coatings in the temperature range 900–1600° C, Acta Mater. 83 (2015) 408-418.
[29] M. Pérez, F.J. Belzunce, A comparative study of salt-bath nitrocarburizing and gas nitriding followed by post-oxidation used as surface treatments of H13 hot forging dies, Surf. Coat. Tech. 305 (2016) 146-157.
[30] S. Veprek, M.G. Veprek-Heijman, The formation and role of interfaces in superhard nc-MenN/a-Si3N4 nanocomposites, Surf. Coat. Tech. 201 (2007) 6064-6070.
[31] R. Zhang, S. Veprek, On the spinodal nature of the phase segregation and formation of stable nanostructure in the Ti–Si–N system, Mat. Sci. Eng. A, 424 (2006) 128-137.
[32] H.T. Kim, C.S. Chae, D.H. Han, D.K. Park, Effect of substrate temperature and input power on TiN film deposition by low-frequency (60 Hz) PECVD, J. Korean Phys. Soc. 37 (2000) 319-323.
[33] M. Orhing, Materials Science of Thin Films: Deposition and Structure, first ed., Academic Press, London, 2001.
[34] D.A. Porter, K.E. Easterling, M. Sherif, Phase Transformations in Metals and Alloys, thrid ed., CRC press, Boca Roton, 2009.